AIP | Journal of Applied Physics

Shape-controlled synthesis and cathodoluminescence properties of elongated α-Fe2O3 nanostructures

M. F. Chioncel, C. Díaz-Guerra, and J. Piqueras

Citation: J. Appl. Phys. **104**, 124311 (2008); doi: 10.1063/1.3054168
View online: http://dx.doi.org/10.1063/1.3054168
View Table of Contents: http://jap.aip.org/resource/1/JAPIAU/v104/i12
Published by the AIP Publishing LLC.

Shape-controlled synthesis and cathodoluminescence properties of elongated α-Fe_2O_3 nanostructures

M. F. Chioncel,[1] C. Díaz-Guerra,[2,a)] and J. Piqueras[2]
[1]*Department of Physics, Faculty of Chemistry, University of Bucharest, Bd. Elisabeta 4-12, 030018 Bucharest, Romania*
[2]*Departamento de Física de Materiales, Facultad de Físicas, Universidad Complutense de Madrid, Ciudad Universitaria s/n, E-28040 Madrid, Spain*

(Received 3 October 2008; accepted 9 November 2008; published online 19 December 2008)

α-Fe_2O_3 (hematite) nanostructures with various morphologies have been grown by thermal oxidation of compacted iron powder at temperatures between 700 and 900 °C. Different thermal treatments have been found to induce the growth of single-crystalline nanowires, nanobelts, nanoplates and featherlike structures, free and caped nanopillars, and pyramidal microcrystals or cactuslike microstructures. The experimental conditions leading to the different morphologies have been systematically investigated, as well as the possible growth mechanisms. The obtained nanostructures have been characterized by scanning electron microscopy (SEM), high-resolution transmission electron microscopy, x-ray diffraction, and cathodoluminescence (CL) spectroscopy in the SEM. The formation of the nanostructures induces changes in the intensity and spectral distribution of the CL emission, as compared with the bulk material. Ligand to metal charge transfer transitions as well as Fe^{3+} ligand field transitions are thought to be involved in the observed luminescence. The evolution of the panchromatic CL intensity in the visible range as a function of temperature shows some anomalies that may be induced by magnetic ordering effects.
 [DOI: 10.1063/1.3054168]

I. INTRODUCTION

Due to size effects and novel physical properties, nanostructures are of great interest both for theoretical studies and nanodevice applications. A large variety of nanostructures, such as nanotubes, nanorods, nanowires, and nanobelts have been synthesized by thermal techniques involving vapor-solid (VS) or vapor-liquid-solid (VLS) mechanisms. In the past years, these nanostructures have become a research field for advanced "bottom-up" nanotechnology. In particular, hematite (α-Fe_2O_3) is of significant scientific and technological importance due to its stability under ambient conditions and dual semiconducting-magnetic properties. Hematite has applications as photocatalyst,[1] gas sensor,[2] and field emission cathode.[3] Its small band gap (~2.1 eV), high resistivity to corrosion, and low cost, make α-Fe_2O_3 suitable as a solar energy conversion material in photoelectrodes as well.[4] Moreover, magnetism of α-Fe_2O_3 nanostructures receives a distinctive attention, as the bulk material presents a first-order magnetic transition at Morin temperature, besides the common Néel transition of antiferromagnetic materials. Its unusual magnetic behavior has been studied extensively in the past decades[5,6] and it has been found that the decrease in the particles to nanosize alters significantly the magnetic behavior of α-Fe_2O_3.[7] Several techniques have been proposed to produce iron oxide nanostructures, including electrodeposition[8] and sol-gel.[9] In addition, several groups have synthesized nanowires of α-Fe_2O_3 by oxidizing bulk iron in a mixed gas ambient.[10–12] However, the growth mechanism is still to be clearly determined. In addition, the optical properties of this oxide, especially luminescence properties, have been scarcely investigated. Actually, luminescence is not commonly observed in the magnetic oxides and appears to require the presence of an impurity that may itself be the emitter or may act to induce emission from the metal ions of the host. Nevertheless, this situation may change when the crystal size is reduced due to surface effects, different defect structure, phonon coupling, and carrier delocalization effects.

In the present work, α-Fe_2O_3 nanostructures have been grown by a thermal treatment of compressed Fe powder under an argon flow. This method was previously reported to lead to the growth of elongated microstructures and nanostructures of different semiconductor oxides,[13–15] but in those works the starting material was the oxide itself, not the metal leading to the corresponding oxide. The influence of the growth parameters, such as temperature, annealing time, and gas flow, on the morphology and properties of the obtained nanostructures has been systematically investigated. The synthesized α-Fe_2O_3 nanostructures have been characterized by scanning electron microscopy (SEM), high-resolution transmission electron microscopy (HRTEM), and x-ray diffraction (XRD), while their luminescence properties were studied by cathodoluminescence (CL) spectroscopy in a SEM.

II. EXPERIMENTAL

The starting material was commercial Fe powder with a nominal purity of 99.9%, purchased from Sigma-Aldrich. The powder was ball milled for 10 h in a centrifugal ball mill (Retsch S100) with 20 mm agatha balls in order to reduce the

a)Electronic mail: cdiazgue@fis.ucm.es.

particle size and to obtain a more homogeneous size distribution. Disk shaped pellets, of about 7 mm in diameter and 2 mm thickness, were prepared by compacting the Fe powder under a compressive load of 1 ton. The pellets were then annealed at different temperatures between 700 and 900 °C for 10 h in a horizontal tube furnace under Ar flow. The treatment temperature was systematically varied in order to find the suitable range inducing the growth of specific nanostructures. At relevant temperatures in this range, argon flow rate and treatment time were also altered to investigate the influence of these parameters over the final geometry of the structures. The thermal treatments consisted of a heating up step (1 h), followed by annealing at a specific temperature and time under Ar flow and cooling to room temperature. However, as the furnace was not sealed for high vacuum conditions, slow oxidation takes place during the thermal treatment, leading to the formation of iron oxide nano- and microstructures. This catalyst-free method leads to the growth of such structures directly on the sample surface, which acts as source as well as substrate for the gas flow favored deposition.

XRD patterns were recorded on a Philips X'Pert PRO diffractometer using Cu $K\alpha$ radiation. Recent works[16] have shown that intensity patterns obtained in XRD and grazing incidence XRD (GIXRD) are usually different for vertically aligned and bent hematite nanowires. For this reason, both geometries have been used in the present work for the structural characterization of our nanostructures. Furthermore, in order to obtain spatially resolved information about the microstructural properties of some samples, x-ray microdiffraction measurements were carried out using a monocapillary with a diameter of 100 μm. Secondary electron images were obtained in a Leica 440 SEM. The CL measurements were carried out at 90 K with a beam energy of 20 keV using a Hitachi S2500 SEM, a Hamamatsu R928P photomultiplier working in the photon counting mode, and a computer controlled Oriel 74100 monochromator. HRTEM images and selected area electron diffraction (SAED) patterns were obtained in a field emission Jeol JEM 3000F microscope operating at 300 kV. For HRTEM observations, nanostructures were released from the disks by sonicating the samples in butanol. Drops of the nanostructures solution were then deposited onto carbon-coated copper grids. Electron beam-induced structural transformations were not observed during these measurements.

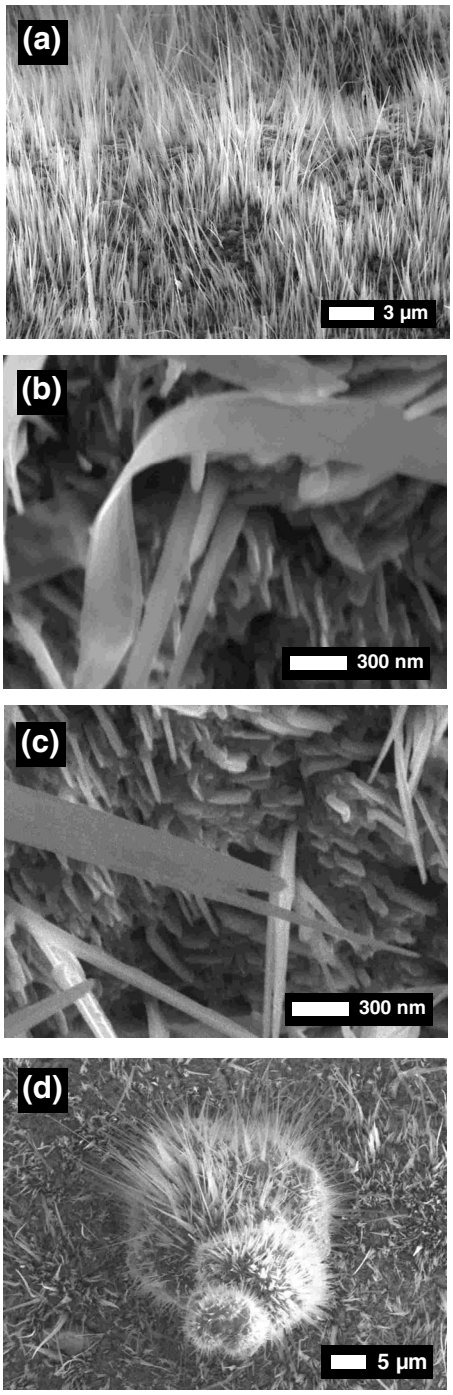

FIG. 1. SEM images of α-Fe_2O_3 nanostructures grown at 730 °C (10 h). (a) Aligned nanowires, [(b) and (c)] nanobelts, and (d) urchinlike structure.

III. RESULTS AND DISCUSSION

After each growth run, the samples were examined in the SEM to determine the influence of the chosen parameters in the growth of the nanostructures. Additional analysis was performed on perpendicular axes of the disks in order to investigate the influence of the Ar flow direction. Also, the lateral surface of the pellets, exposed perpendicularly to the Ar flow (compared with the almost parallel exposure of the upper surface of the pellet) was investigated in order to understand if the flow direction alters significantly the morphology of the sample. No such variation was observed.

Different nano- and microstructures, whose morphology and distribution depend on the specific annealing treatment applied, were found to grow on the surface of the pellets. Annealing in the temperature range of 700–730 °C for 10 h causes the growth of high density of narrow nanowires [Fig. 1(a)] with diameters of 100–200 nm and lengths of about 10 μm, as well as rods and, rarely, flakes. The nanowires, which tend to grow thinner, longer, and with high density toward the border of the sample, cover entirely the pellet and are aligned in a dense array, approximately perpendicular to the substrate surface. Most of the α-Fe_2O_3 nanowires have uniform size along their entire lengths and terminate at a sharp tip. Wider needles have, however, decreasing width

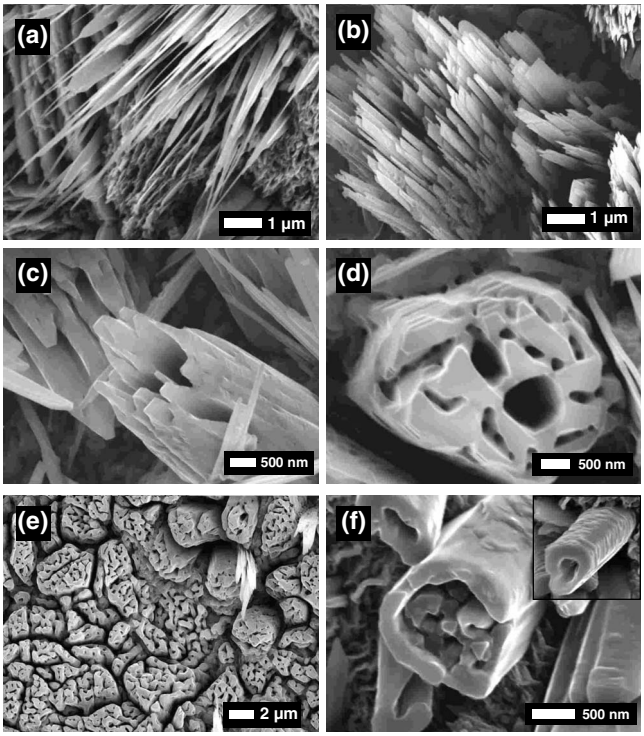

FIG. 2. SEM micrographs of nanostructures and microstructures grown in the 770–830 °C temperature range (10 h). Bundles of (a) nanoneedles and (b) flakes grown near the [(c) and (d)] edge of a sample at 830 °C. Different tubular structures obtained at 770 °C. (e) Distribution of tubular structures covering large areas of a sample grown at 770 °C. (f) Wide tubular structure filled with triangular pillars (800 °C) and hollow narrower tube (inset).

from the base to the tip. In the central part of these samples, long nanowires, occasionally bended, and nanobelts are evenly distributed over the background surface, which shows a domainlike or porous appearance. The nanobelts have thickness of about 20 nm [Fig. 1(b)]. Pointed tips of some of these belts suggest that they may be formed by adjoined wires [Fig. 1(c)]. Some microspheres showing porous walls with protruding nanorods and nanoneedles grow in the nanowire-rich areas as well. Figure 1(d) shows such urchin-like structure with nanoneedles pointing radially outward normal to the surface.

In samples treated at temperatures in the range of 750–830 °C, SEM images reveal the presence of nanowires slightly thicker, 150–250 nm, than those grown in the previous temperature range. In addition, nanoneedles are observed in some regions, mainly near the edge of the sample, while different structures, as pillars and tubes, grow in the central part. The needles tend to aggregate during these treatments and form bundles and flakes, as Fig. 2(a) and 2(b) shows. The observed tubular structures appear to be in different stages of formation. Actually, the structure of the tube shown in Fig. 2(c) suggests that it is formed by aggregation of plates or of bundles of needles, while the morphology of the complex tubular structure shown in Fig. 2(d) cannot be directly related to the needles. The tubular structures usually cover large areas of the sample, giving rise to the cortex appearance shown in Fig. 2(e). The larger tubular structures appear, mainly in samples treated at 800–830 °C, filled with pillars of triangular section with side of less than 200 nm

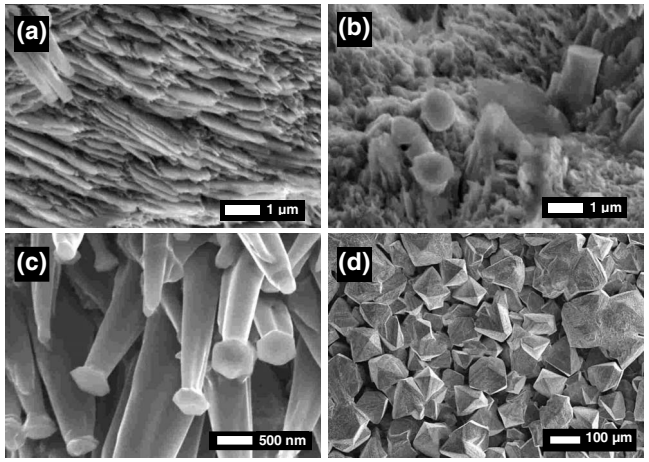

FIG. 3. [(a)–(c)] SEM images showing the influence of growth time on the morphology of the structures synthesized at 830 °C. (a) Nanoplates and (b) incipient columnar structures with flat top are found in samples treated for 3 h. (c) Longer columnar structures with hexagonal heads can be observed in samples treated for 10 h. (d) Octahedral crystals grown at 900 °C (10 h).

[Fig. 2(f)], while narrower tubes have hollow end. The stratified appearance of the lateral walls suggests that they grow from superposition of hollow cave polyhedra.

In the series of samples treated at 830 °C for different times, the influence of annealing time on the final morphology of the structures is observed. In addition to the above-described nanowires or nanoneedles and the tubular structures, the nanoplates shown in Fig. 3(a) grow during the 3 h treatment. Also, incipient columnar structures with a flat top, as those shown in Fig. 3(b), are observed. After the 10 h treatment the columns appear well developed with a hexagonal, hatlike, top [Fig. 3(c)]. The cortex structure is the main feature in samples annealed for 15 h. By annealing at 900 °C no nanostructures were found to grow, and the sample consists of defined octahedral microcrystals as prevalent morphology [Fig. 3(d)].

The present results reveal that the most homogeneous distribution of nanostructures is obtained after the 700–730 °C treatments, which lead to the growth of nanowires all over the surface of the disk, while at higher temperatures distributions of different structures such as nanoneedles, tubes, and rods, are obtained. In order to associate physical properties to specific nanostructures, the CL measurements were performed preferently on such samples, containing a dense distribution of nanowires. Moreover, the small diameter of the nanowires enabled their observation by HRTEM without special specimen preparation.

Nanowires of the samples treated at 730 or 800 °C were observed by HRTEM following the above-described method. Similar results were obtained in nanowires from the two samples. Figure 4(a) shows a 190 nm wide nanowire grown on a sample treated at 800 °C. Figure 4(b) is a detailed micrograph of the area marked in the previous image, showing fringes running perpendicular to the edge of the nanowire. The corresponding SAED pattern, shown in the inset, can be identified as the (001) pattern of α-Fe_2O_3. The HRTEM image shown in Fig. 4(c) reveals that the fringe spacing measures 0.251 nm, which corresponds to the (110) interplanar spacing. This indicates the single crystalline nature of the

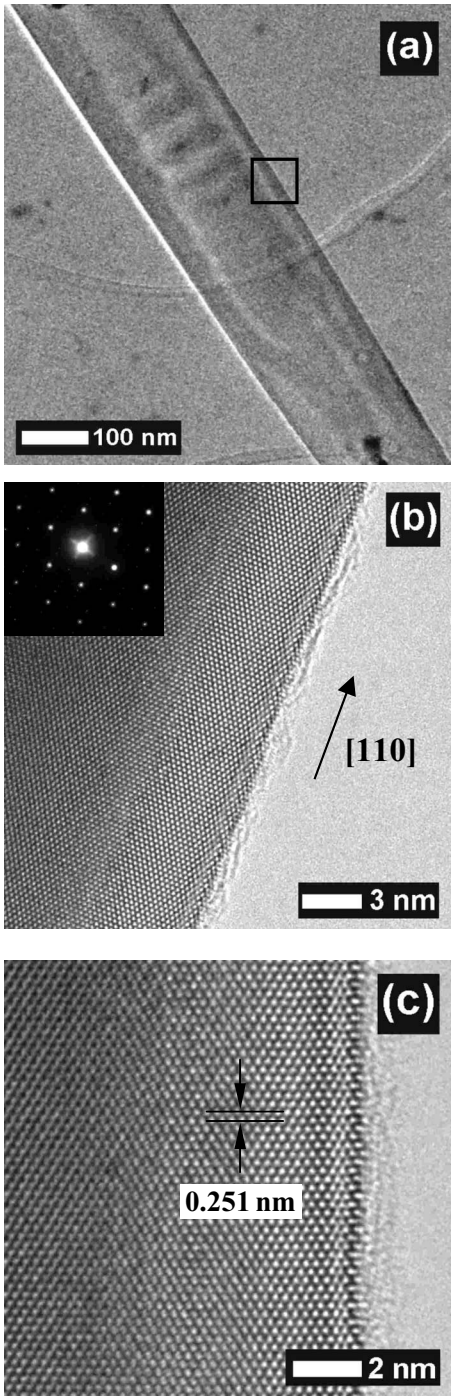

FIG. 4. (a) Low magnification TEM micrograph of a hematite nanowire grown at 800 °C. (b) HRTEM image of the area marked in the previous micrograph. The corresponding SAED pattern, shown in the inset, can be identified as the (001) pattern of α-Fe_2O_3. (c) HRTEM micrograph of the same nanowire showing the (110) interplanar spacing of this material.

wires that grow along the [110] direction. TEM measurements carried out in a number of nanowires indicate that this is the usual growth direction of our nanostructures. It should be mentioned that careful examination of the obtained SAED patterns frequently revealed the existence of weak extra spots. These superstructures have been previously observed in SAED patterns of both hematite nanowires[12] and microcrystals[17] and were attributed to oxygen vacancies in the first case and to different distribution of iron vacancies in the second one.

XRD and GIXRD patterns show strong and sharp diffraction peaks that can be unambiguously indexed to rhombohedral α-Fe_2O_3 (a=5.038 Å, c=13.772 Å), evidencing that the as-prepared nanostructures are well crystallized. A dominant peak, corresponding to the (110) reflection, and less intense (300) and (220) peaks can be observed in micro-XRD patterns from samples where the nanowires and nanobelts prevail (700–750 °C), as shown in Fig. 5(a). When measurements are performed in nanowire-rich specific areas of the samples treated at slightly higher temperatures, e.g., 770 °C, the micro-XRD [Fig. 5(b)] patterns show a significant reduction in the intensity of the (300) reflection. It has been recently reported[16] that contribution to the (110) peak arises from straight hematite nanowires oriented vertically and from the vertical portion of the bent nanowires, whereas contribution to the (300) peak arises from bent nanowires when (300) planes become parallel to the substrate as a result of bending. The intensity of the (110) peak increases and that of (300) reflection decreases with vertical alignment of nanowires in the XRD pattern. Hence, our XRD results agree with the above-described SEM observations, which show that elongated nanostructures grown at intermediate temperatures (770 °C) are slightly thicker and shorter than those grown at lower temperatures (700–730 °C). Bending of the nanostructures is then more difficult in the former case as compared with the latter, which explains the differences observed between both XRD patterns. The higher relative intensity of the (110) diffraction peak indicates that [110] is the preferential nanowire growth direction, in agreement with our HR-TEM results and other studies of α-Fe_2O_3 nanowires and nanobelts grown by thermal oxidation of iron.[18,19] Such preferential orientation is progressively lost when the treatment temperature is increased and wider structures with other morphologies begin to grow on the surface of the pellets. In particular, the relative weight of the (116) and especially the (104) reflections increases in XRD patterns [Fig. 5(c)] of nanostructures grown at 800–850 °C, as the pillars and tubular structures shown in Fig. 2. These results agree with those reported by Jia *et al.*[20] in XRD patterns of hematite nanotubes and tube-in-tube nanostructures[21] grown by hydrothermal methods.

Regarding the growth mechanism of our nanostructures, it has been generally accepted that synthesis of α-Fe_2O_3 nanowires by iron oxidation is governed neither by the VLS process nor the VS process,[11] which are the two commonly accepted mechanisms for the growth of nanowires in the gas phase. Takagi[22] initially showed that α-Fe_2O_3 whiskers grow from the tip rather than extrusion from the oxidized substrate, so that the hematite nanostructures grow by Fe surface or internal diffusion (tip growth mechanism). Surface diffusion mechanisms were proposed to account for the growth of α-Fe_2O_3 nanoflakes,[23] bicrystalline hematite nanowires,[24] and aligned arrays of hematite nanowires as well.[11] In particular, the supply of iron atoms for α-Fe_2O_3 nanowires growth has been considered to take place by surface diffusion along the sides of the nanowire and internal diffusion along planar defects up the axis of the nanowire.[11] Nevertheless, a mechanism involving VLS phase was also suggested for the growth of α-Fe_2O_3 nanowires.[25] Previous investiga-

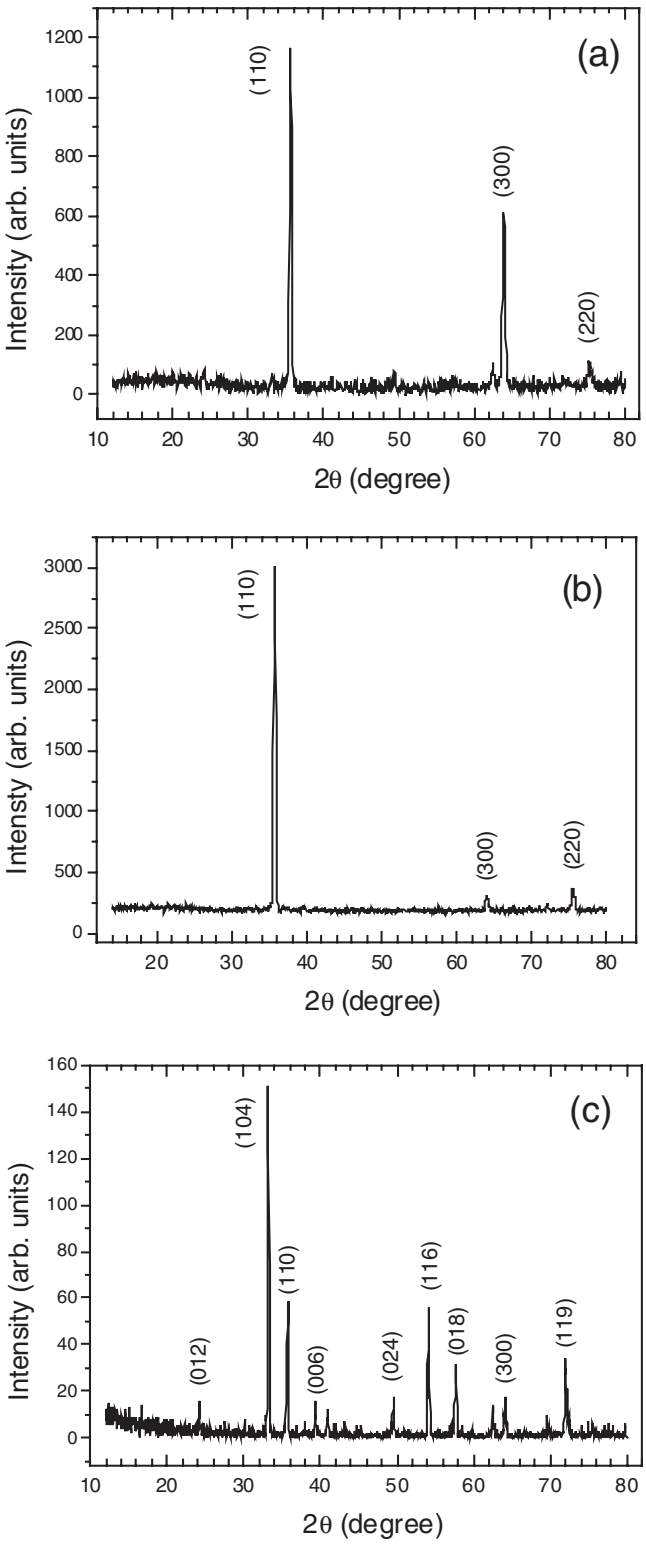

FIG. 5. Micro-XRD patterns of samples treated for 10 h at different temperatures: (a) 730 °C and (b) 770 °C. In both cases, measurements were performed in regions containing a high density of aligned nanowires. (c) 800 °C. The diffractogram corresponds to the central area of the sample, containing a high density of tubular structures as those shown in Fig. 2.

tion of α-Fe_2O_3 nanobelts and nanowires[11] revealed that low-temperature synthesis leads to the formation of nanobelts, while higher temperatures favor the growth of nanowires. No such observation is confirmed by our results. The differences observed in the morphology of the nanostructures grown near the edge and at the center of several samples appear to be related to surface energy and different growth rates along different crystal directions. Besides the morphological diversity, there is a clear distinction in the relative alignment of the nanowires grown at the edge and in the center of the pellet. The nanowires grown toward the edge of the pellet are very dense and vertically aligned, while in the central part they frequently grow grouped in bunches leading to an inflorescencelike appearance. They may also grow vertically on top of spherical/oval microstructures, creating cactus/urchinlike morphologies. High surface density of the as-growing nanostructures and strong van der Waals forces between them may be considered in some situations as responsible for the aligned growth.[26] In our case, SEM observations carried out in pellets covered by Fe powder prior to the annealing treatment actually suggest that the alignment may be induced by overcrowding, which limits the possibility of nanowire growth in other directions.[27] A higher density of nucleation sites will then promote a higher degree alignment of the as-grown nanowires due to overcrowding. In the central areas, characterized by a less homogeneous morphology, nanostructures are all grown out of the pellet surface; no nanobelts or nanoneedles are nucleated on the well-crystallized flakes. This likely indicates that the nanostructures grow from planar defects, such as grain boundaries and twins, while surface diffusion provides transport of Fe and O for the growth of α-Fe_2O_3 nanowires.[18] A similar surface diffusion scenario to that formulated by Han *et al.*[28] for the formation of needle-tip, large-tip and bamboolike α-Fe_2O_3 nanowires—involving Fe diffusion from the bottom to the tip—may be effective for the growth of the atypical hematite morphologies observed in our samples. Moreover, our XRD data indicate [110] as the preferential growth direction in samples where the nanowire morphology is dominant. It is known that Fe atoms are more reactive and more deficient in the (110) plane,[11] so that the iron diffusion and the nanowire growth along the [110] direction are favored. Hence, the existence of the preferential nanowire growth along the [110] axis also supports a surface diffusion growth mechanism. In addition, several other aspects suggest that VS or VLS processes do not play a significant role in the growth mechanism of the grown α-Fe_2O_3 nanowires. In our thermal treatment, no catalysts have been used, the synthesized nanowires grow directly on the local iron substrate, the treatment time is rather long and the evaporation may be negligible since the temperature employed is much lower than the melting points of iron and α-Fe_2O_3 (1535 and 1350 °C, respectively).

Optical emission properties of α-Fe_2O_3 have been scarcely investigated likely due to its low quantum efficiency. For instance, photoluminescence (PL) emission is hardly observed in this material due to resonant energy transfer between cations and lattice, local forbidden *d-d* transitions, and magnetic relaxations.[29] Nevertheless, crystal size reduction may induce an increase in luminescent emission through several mechanisms such as loss of ferromagnetic long-range order leading to reduction in magnetic interactions, altered density of the electronic population in the valence band and simultaneous enhancement of electron-phonon coupling and carrier delocalization induced by a

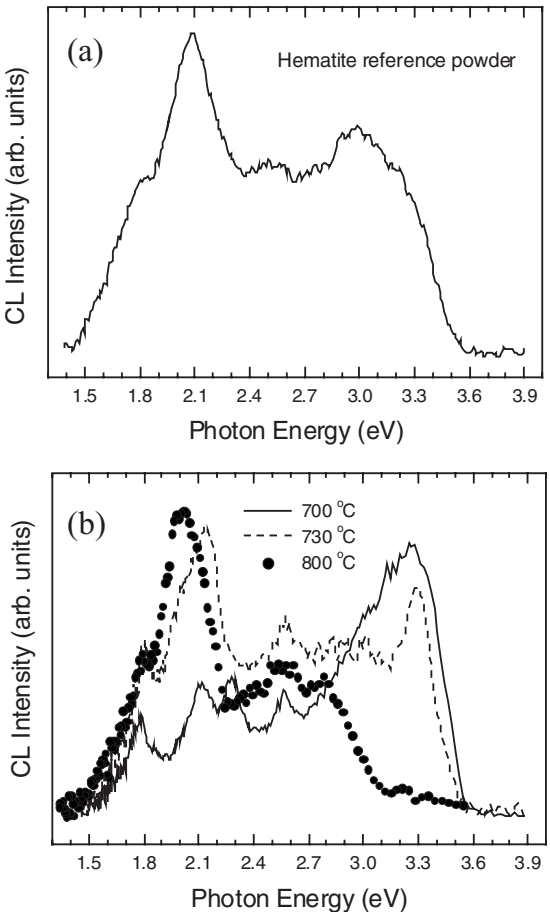

FIG. 6. (a) CL spectrum of untreated α-Fe_2O_3 powder. (b) CL spectra of α-Fe_2O_3 nanowires grown at three different temperatures: 700, 730, and 800 °C. Measurements were carried out at 90 K using a 20 kV accelerating voltage.

significant decrease in energy transfer between ions.[29,30] The CL spectrum of reference, untreated, α-Fe_2O_3 powder [Fig. 6(a)] shows a complex emission in the visible range, with two clearly resolved bands peaked at about 2.09 and 3.0 eV. Besides, weaker shoulders centered near 1.83, 2.50, and 3.23 eV can be also appreciated. Measurements performed on our thermally treated samples indicate that the grown morphology alters the spectral distribution of the CL emission [Fig. 6(b)]. The shoulder previously found at about 1.83 eV can be observed as a resolved band centered at (1.79–1.81) eV, while two other resolved CL bands peaked at about 2.28 and 2.56 eV can be observed as well. Further changes, as the appearance of an enhanced CL emission at about (3.25–3.30) eV, can be appreciated in the high energy range of CL spectra of samples uniformly covered with a high density of nanowires or nanobelts (those grown at 700–750 °C).

The existence of optical transitions in the same spectral range than our CL bands has been reported in several absorption investigations of α-Fe_2O_3.[30–32] These transitions have been also studied by correlation between absorption and spectrally resolved photocurrent measurements carried out in hematite thin films.[30] The absorption bands have been related to ligand field transitions of Fe^{3+} ions in octahedral coordination (*d-d* transitions), pair excitations resulting from the magnetic coupling of adjacent Fe^{3+} cations (double exciton processes) and ligand to metal charge transfer (LMCT) transitions. In the 4.96–3.10 eV spectral range, absorption is related to LMCT transitions—that can roughly be thought of as representing a charge transfer from the oxygen to the iron ions—and partly to the contributions of the Fe^{3+} ligand field transitions. In the 3.10–2.07 eV range, absorption is related to pair excitation processes, possibly overlapped with the $^6A_1 \rightarrow {}^4E$ and $^4A_1$ (^4G) ligand field transition and the charge-transfer band tail, while in the 2.07–1.38 eV interval, different ligand field transitions prevail.[30–32] It was reported[33] that the crystal size has little effect on the absorption bands in the first and latter intervals while bands in the second spectral range (3.10–2.07 eV) blueshift with reducing size.

Our CL measurements (Fig. 6) show a weak emission centered at about 1.8 eV in the low energy side of the spectra. Similar weak emission in the (1.70–1.83) eV range has been previously reported in PL measurements carried out in hematite nanocrystals and attributed to the $^6A_1 \rightarrow {}^4T_2$ (^4G) ligand field transition.[29] The CL peak centered between 2.01 and 2.14 eV, depending on the sample considered, is related to the hematite optical band gap. It is well accepted that the band edge of α-Fe_2O_3 is located in the range of (2.00–2.20) eV.[34–36] The transitions in this energy region include the *d-d* transitions, pair excitation, and less charge transfer, and the former two transitions mainly come from the narrow *d* bands, so the optical properties of hematite band edge cannot be accounted for intrinsic semiconductor. Han *et al.*[37] recently reported room temperature PL of α-Fe_2O_3 nanowires with a band gap of 2.14 eV, while PL spectra from capped and naked α-Fe_2O_3 nanocrystals indicate band gaps in the 1.93–2.12 eV range.[29,38] Besides, the investigation of size-dependent optical properties of α-Fe_2O_3 nanorods (20–40 nm wide) showed a clear blueshift of the absorption edge, up to 2.65 eV, as the size of these nanostructures decreased.[39] Such large shifts have not been observed in our CL measurements. However, small blueshifts (from 2.01 eV to 2.14 eV) are observed in emission from nanowires. For instance, this shift can be observed when CL spectra recorded in samples grown at 700–730 °C [Fig. 6(b)], containing a high density of long and thin nanowires, are compared with spectra from the edge regions of the samples treated at 800 °C, where bundles of shorter nanowires and flakes were observed. PL emissions at energies higher than the optical band gap were previously reported in hematite spindle-shaped nanoparticles with average dimensions of 1×5 nm^2.[40] The PL bands centered at about 3.1, 2.70, and 2.3 eV were not attributed to quantum confinement effects but to LMCT transitions. We suggest that this is the origin of our CL bands peaked near 2.56, 3.0, and 3.25 eV, although the contribution of Fe^{3+} ligand field transitions cannot be ruled out.

Total CL intensity versus temperature was measured between 90 and 300 K in samples where a high density of uniformly distributed nanowires of similar size and morphology were observed, as those treated for 10 h at 700 and 730 °C. The evolution of the panchromatic CL intensity in the visible range of two of the samples as a function of temperature is shown in Fig. 7. The expected decrease in the CL signal with increasing temperature, due to the enhancement in nonradiative processes, is altered in the temperature

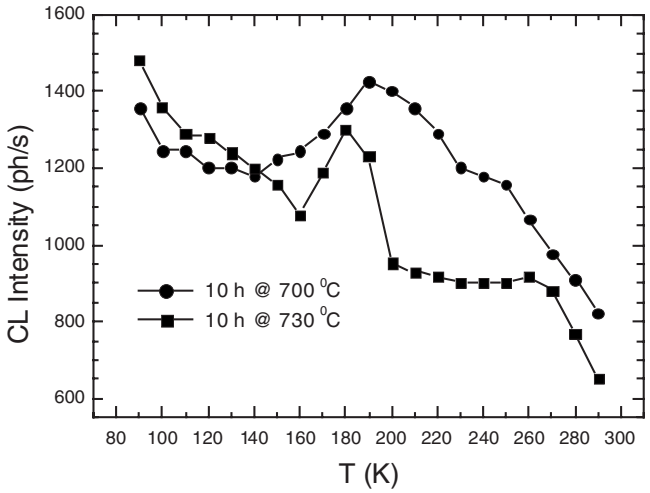

FIG. 7. Temperature dependence of the CL intensity measured in α-Fe_2O_3 nanowires grown at 700 and 730 °C.

range of 170–210 K, showing a peak at around 180–190 K. The appearance of this maximum in the mentioned temperature range has been found to be reproducible in different runs and different samples. We suggest that this peculiar behavior could have the same physical origin than the luminescence anomalies reported in several other antiferromagnetic compounds.[41–44] Bulk α-Fe_2O_3 is well known as an antiferromagnetic material with a Néel temperature (T_N) of 950 K. At Morin temperature, $T_M \sim 263$ K (Ref. 45) the bulk material presents a first-order magnetic transition. Below T_M, two magnetic sublattices are oriented along the rhombohedral [111] axis (c-axis) and are exactly antiparallel, inducing a uniaxial antiferromagnetic behavior. Above T_M, α-Fe_2O_3 displays weak ferromagnetism due to incomplete antiparallelism of the spins, created by a slight spin canting of the two magnetic sublattices.[46] Size reduction to nanometer scale induces significant alteration of the hematite magnetic properties. In fact, polycrystalline wires 200 nm in diameter were reported to have T_M=80 K and T_N=350 K,[47] while a T_M value of 125 K was reported for single-crystalline nanowires.[19]

Anomalies of the luminescence intensity with temperature have been reported in several antiferromagnetic compounds. In particular, Holloway *et al.*[41–43] reported changes in the luminescence of MnF_2 and alkali manganese trifluorides at temperatures of about $T_N/2$ and T_N. The luminescence behavior of these materials was explained within the framework of the vibronic-state model, the observed T_N alterations being attributed to the magnetic ordering that influences the Stokes shift through a magnetoelastic effect. The observed strong luminescence alterations at $T_N/2$ were not related to any crystal cooperative phenomena and were attributed to a coupling effect between local magnetic ordering of the excited Mn^{2+} ions that become aligned with respect to surrounding lattice, and lattice distortion which causes a condensation in the thermal excitation of the magnetic local mode. Temperature dependent anomalies in the cathodoluminescence of the antiferromagnetic oxides NiO, CoO,[44] and oxygen-deficient $YBa_2Cu_3O_{7-x}$ (Ref. 48) were also reported as appearing at about one-half of the Néel temperature and were explained by magnetic ordering effects, within the frame of the Holloway model. The magnetic behavior of the grown α-Fe_2O_3 nanostructures is currently under investigation to confirm our hypothesis that the physical nature of the observed alteration of the CL panchromatic emission is related to magnetic ordering effects, similarly observed in the abovementioned antiferromagnetic systems.

IV. CONCLUSIONS

In summary, thermal treatment of compacted Fe powder under Ar flow in the temperature range (700–900) °C leads to the formation of α-Fe_2O_3 nanostructures and microstructures with different morphologies, such as nanowires, nanobelts, nanoneedles, micro- and nanotubes, nanowide flakes, featherlike structures, and well shaped pyramidal microcrystals. Diffusion processes seem to play a key role in the growth mechanism of the obtained nanostructures. In the samples with dominant nanowire morphology (700–750 °C), the nanowires grow preferentially along the [110] direction, as confirmed by XRD and HRTEM measurements. Size effects in the grown structures lead to an increase in the CL intensity and induce changes in the spectral distribution of the emission, as compared with bulk α-Fe_2O_3. Ligand to metal charge transfer transitions as well as Fe^{3+} ligand field transitions are thought to be involved in the observed luminescence. CL intensity of the nanowires as a function of temperature shows some anomalies in the range of 170–210 K that may be induced by magnetic ordering effects.

ACKNOWLEDGMENTS

This work has been supported by MEC through Project No. MAT2006-01259. M.F.C. acknowledges the financial support received from UCM and Banco Santander.

[1] A. Kay, I. Cesar, and M. Grätzel, J. Am. Chem. Soc. **128**, 15714 (2006).
[2] L. Huo, W. Li, L. Lu, H. Cui, S. Xi, J. Wang, B. Zhao, Y. Shen, and Z. Lu, Chem. Mater. **12**, 790 (2000).
[3] Y. W. Zhu, T. Yu, C. H. Sow, Y. J. Liu, A. T. Wee, X. J. Xu, C. T. Lim, and J. T. L. Thong, Appl. Phys. Lett. **87**, 023103 (2005).
[4] T. Ohmori, H. Takahashi, H. Mametsuka, and E. Suzuki, Phys. Chem. Chem. Phys. **2**, 3519 (2000).
[5] M. Catti, G. Valerio, and R. Dovesi, Phys. Rev. B **51**, 7441 (1995).
[6] M. F. Hansen, C. B. Koch, and S. Mørup, Phys. Rev. B **62**, 1124 (2000).
[7] D. S. Xue, C. X. Gao, Q. F. Liu, and L. Y. Zhang, J. Phys.: Condens. Matter **15**, 1455 (2003).
[8] B. Zong, Y. Wu, G. Han, B. Yang, P. Luo, L. Wang, J. Qiu, and K. Li, Chem. Mater. **17**, 1515 (2005).
[9] Y. Lu, Y. Yin, B. T. Mayers, and Y. Xia, Nano Lett. **2**, 183 (2002).
[10] Y. Fu, J. Chen, and H. Zhang, Chem. Phys. Lett. **350**, 491 (2001).
[11] X. G. Wen, S. H. Wang, Y. Ding, Z. L. Wang, and S. Yang, J. Phys. Chem. B **109**, 215 (2005).
[12] Y. L. Chueh, M. W. Lai, J. Q. Liang, L. J. Chou, and Z. L. Wang, Adv. Funct. Mater. **16**, 2243 (2006).
[13] C. Díaz-Guerra and J. Piqueras, J. Appl. Phys. **102**, 084307 (2007).
[14] P. Hidalgo, B. Méndez, and J. Piqueras, Nanotechnology **18**, 155203 (2007).
[15] E. Nogales, B. Méndez, and J. Piqueras, Nanotechnology **19**, 035713 (2008).
[16] U. P. Deshpande, T. Shripathi, D. Jain, A. V. Narlikar, S. K. Deshpande, and Y. Y. Fu, J. Appl. Phys. **101**, 064304 (2007).
[17] M. Boudeulle, H. Batis-Landoulsi, C. H. Leclercq, and J. Vergnon, Solid State Chem. **48**, 21 (1983).
[18] Y. Y. Fu, J. Wang, J. Chen, Y. Yan, A. V. Narlikar, and H. Zhang, Chem.

Phys. Lett. **379**, 373 (2003).
[19]C. H. Kim, H. J. Chun, D. S. Kim, J. Park, J. Y. Moon, G. Lee, J. Yoon, Y. Jo, M. Jung, S. I. Jung, and C. J. Lee, Appl. Phys. Lett. **89**, 223103 (2006).
[20]C. J. Jia, L. Sun, Z. Yan, L. You, F. Luo, X. Han, Z. Zhang, Y. Pang, and C. Yan, Angew. Chem., Int. Ed. **44**, 4328 (2005).
[21]C. J. Jia, L. Sun, Z. Yan, Y. Pang, L. You, and C. Yan, J. Phys. Chem. C **111**, 13022 (2007).
[22]R. Takagi, J. Phys. Soc. Jpn. **12**, 1212 (1957).
[23]Z. Zheng, Y. Chen, Z. Shen, J. Ma, C. Sow, W. Huang, and T. Yu, Appl. Phys. A: Mater. Sci. Process. **89**, 115 (2007).
[24]R. Wang, Y. Chen, Y. Fu, H. Zhang, and C. Kisielowski, J. Phys. Chem. B **109**, 12245 (2005).
[25]T. Yu, Y. Zhu, X. Xu, K. Yeong, Z. Shen, P. Chen, C. Lim, J. Thong, and C. Sow, Small **2**, 80 (2006).
[26]S. Fan, M. G. Chapline, N. R. Franklin, T. W. Tombler, A. M. Cassell, and H. J. Dai, Science **283**, 512 (1999).
[27]W. S. Shi, H. Y. Peng, Y. F. Zheng, N. Wang, N. G. Shang, Z. W. Pan, C. S. Lee, and S. T. Lee, Adv. Mater. (Weinheim, Ger.) **12**, 1343 (2000).
[28]Q. Han, Y. Y. Xu, Y. Y. Fu, H. Zhang, R. M. Wang, T. M. Wang, and Z. Y. Chen, Chem. Phys. Lett. **431**, 100 (2006).
[29]B. S. Zou and V. Volkov, J. Phys. Chem. Solids **261**, 2757 (2000).
[30]L. A. Marusak, R. Messier, and W. B. White, J. Phys. Chem. Solids **41**, 981 (1980).
[31]D. M. Sherman and T. D. Waite, Am. Mineral. **70**, 1262 (1985).
[32]Y. P. He, Y. M. Miao, C. R. Li, Q. Wang, L. Cao, S. S. Xie, G. Yang, B. S. Zou, and C. Burda, Phys. Rev. B **71**, 125411 (2005).
[33]J. Wang, W. B. White, and J. H. Adair, Mater. Lett. **60**, 2013 (2006).
[34]P. Merchant, R. Collins, R. Kershaw, K. Dwight, and A. Wold, J. Solid State Chem. **27**, 307 (1979).
[35]A. A. Akl, Appl. Surf. Sci. **233**, 307 (2004).
[36]S. Mitra, S. Das, K. Mandal, and S. Chaudhuri, Nanotechnology **18**, 275608 (2007).
[37]Q. Han, Z. Liu, Y. Xu, Z. Chen, T. Wang, and H. J. Zhang, PhysChemComm **111**, 5034 (2007).
[38]B. S. Zou, W. Huang, M. Y. Han, S. Li, X. Wu, Y. Zhang, J. Zhang, P. Wu, and R. Wang, J. Phys. Chem. Solids **58**, 1315 (1997).
[39]S. Zeng, K. Tang, and T. Li, J. Colloid Interface Sci. **312**, 513 (2007).
[40]N. J. Cherepy, D. B. Liston, J. A. Lovejoy, H. Deng, and J. Z. Zhang, J. Phys. Chem. B **102**, 770 (1998).
[41]W. W. Holloway, M. Kestigian, R. Newman, and E. W. Prohofsky, Phys. Rev. Lett. **11**, 82 (1963).
[42]W. W. Holloway and M. Kestigian, Phys. Rev. Lett. **13**, 235 (1964).
[43]W. W. Holloway, E. W. Prohofsky, and M. Kestigian, Phys. Rev. **139**, A954 (1965).
[44]C. Díaz-Guerra and J. Piqueras, Solid State Commun. **104**, 763 (1997).
[45]N. Amin and S. Arajs, Phys. Rev. B **35**, 4810 (1987).
[46]C. G. Shull, W. A. Strauser, and E. O. Wollan, Phys. Rev. **83**, 333 (1951).
[47]L. Y. Zhang, D. S. Xue, X. F. Xu, A. B. Gui, and C. X. Gao, J. Phys.: Condens. Matter **16**, 4541 (2004).
[48]P. Gómez, J. Piqueras, M. J. Sayagués, and J. M. González-Calbet, Solid State Commun. **96**, 45 (1995).